INTERNATIONAL JOURNAL FOR NUMERICAL AND ANALYTICAL METHODS IN GEOMECHANICS
Int. J. Numer. Anal. Meth. Geomech., **23**, 1215–1243 (1999)

FORMULATION OF A UNIFIED CONSTITUTIVE MODEL FOR CLAYS AND SANDS

JUAN M. PESTANA[1]* AND ANDREW J. WHITTLE[2]

[1]*University of California, Berkeley, CA, U.S.A.*
[2]*Massachusetts Institute of Technology, Cambridge, MA, U.S.A.*

SUMMARY

This paper presents a new generalized effective stress model, referred to as MIT-S1, which is capable of predicting the rate independent, effective stress–strain–strength behaviour of uncemented soils over a wide range of confining pressures and densities. Freshly deposited sand specimens compressed from different initial formation densities approach a unique condition at high stress levels, referred to as the limiting compression curve (LCC), which is linear in a double logarithmic void ratio, e, mean effective stress space, p'. The model describes irrecoverable, plastic strains which develop throughout first loading using a simple four-parameter elasto-plastic model. The shear stiffness and strength properties of sands in the LCC regime can be normalized by the effective confining pressure and hence can be unified qualitatively, with the well-known behaviour of clays that are normally consolidated from a slurry condition along the virgin consolidation line (VCL). At lower confining pressures, the model characterizes the effects of formation density and fabric on the shear behaviour of sands through a number of key features: (a) void ratio is treated as a separate state variable in the incrementally linearized elasto-plastic formulation: (b) kinematic hardening describing the evolution of anisotropic stress–strain properties: (c) an aperture hardening function controls dilation as a function of 'formation density'; and (d) the use of a single lemniscate-shaped yield surface with non-associated flow. These features enable the model to describe characteristic transitions from dilative to contractive shear response of sands as the confining pressure increases. This paper summarizes the procedures used to select input parameters for clays and sands, while a companion paper compares model predictions with measured data to illustrate the model capability for describing the shear behaviour of clays and sands.

KEY WORDS: constitutive relations; sands; clays; elastoplasticity; bounding surface plasticity

1. INTRODUCTION

The formulation and evaluation of constitutive models which can simulate reliably the complex stress–strain–strength behaviour of soils is an iterative process which attempts to extend predictive capabilities, while controlling complex such that input parameters are clearly defined. Previous research at MIT has led to the development of a series of generalized effective stress models for clays based on the theory of incrementally linearized elasto-plasticity. The most recent version, MIT-E3,[1] describes the rate independent behaviour of normally to moderately

* Correspondence to: Juan M. Pestana-Nascimento, Geotechnical Engineering, Department of Civil and Environmental Engineering, 440 Davis Hall-1710, Berkeley, CA 94720-1710, U.S.A. E-mail: Pestana@CE.Berkeley.edu

CCC 0363–9061/99/121215–29$17.50
Received June 1998
Revised 20 November 1998

overconsolidated clays (OCR $\leqslant 8$) and achieves high-quality predictions of measured anisotropic stress–strain properties of K_0-consolidated clays in a variety laboratory shear tests.[2] This model has also been applied in finite element analyses of several practical geotechnical problems.[3,4] This paper presents the formulation of a new effective stress model, referred to as MIT-S1, that can describe the behaviour of sands, silts and clays within a single framework. Examples show that the new model greatly extends the productive capabilities of its predecessor but actually requires fewer input parameters.

Most of the existing constitutive models for clays are based on the conceptual framework of critical state soil mechanics, that was originally developed from laboratory data for specimens that are resedimented from a slurry condition. To a first approximation, the rate-independent consolidation behaviour can be described by a virgin consolidation line (VCL) that is linear when plotted in a void ratio-logarithmic effective stress space (e-log p', where p' is the mean effective stress). Elasto-plastic models were first introduced by comparing the compression behaviour along the VCL with the strains occurring during unloading and reloading.[5] A second key observation was that when sheared (under a variety of stress paths and drainage conditions), the clays eventually reached a critical state where continued distortions took place at constant effective stress and void ratio (i.e. no further volume change), as originally suggested by Casagrande.[6] For resedimented clays, the critical state can be projected as a locus parallel to the VCL (in e-log p' space). According to the critical state framework, there is then a unique state boundary surface which defines the limits of possible states (i.e. e, p', q; in triaxial stress space) for shearing of normally consolidated clay specimens.[7] Their strength and deformation properties are then proportional to the effective consolidation stress, while effects of overconsolidation can be related to the strains that occur during swelling (and are also constrained by the state boundary surface). These concepts of normalized behaviour have important implications in the measurement of clay properties,[8] while there is no independent effect of void ratio on the strength and stiffness of normally consolidated clays (however, void ratios does affect the peak strength of overconsolidated clays according to Hvorslev's criterion). Limitations of the basic framework of critical state soil mechanics, such as the development of anisotropic stress–strain–strength properties for K_0-consolidated soils, are also well documented and have been addressed in the formulation of more comprehensive soil models.[9–11]

In contrast to the sedimentation of clays, sands can be deposited at a range of initial formation densities, and their stress–strain–strength properties are functions of both the confining pressure and density (barotropic and pycnotropic effects[12]), as well as other factors relating to the depositional fabric. Most of the existing elasto-plastic models for sands suffer from two major limitations:

1. Although it is generally accepted that some measure of density (void ratio, relative density, etc.) should be included as a state variable in representing the behaviour of cohesionless soils, most existing models have material input parameter that depend on density (and/or confining pressure). This situation arises in formulations which assume that the yield surface, peak friction angle and dilatancy rates are functions of the initial density (e.g. loose, dense). As a result, the stress–strain–strength properties of a given sand at two different initial states (confining pressure or density) are characterized as two separate materials with different sets of input parameters. Improved modelling of sand behaviour can be achieved by introducing void ratio in the formulation through a normalizing state parameter (after Been and Jefferies;[13] $\psi = (e - e_{cs})$, where e is the current void ratio and e_{cs} is the critical state void ratio at the

current mean effective stress) as used in the formulation of 'Nor sand' by Jefferies.[14] However, this approach relies on accurate estimation of the critical state line and can only be achieved through extensive (and high-quality) laboratory measurements of critical state conditions from drained and undrained shear tests. Apart from the difficulty in making these measurements, the data show that the critical state line is non-linear (in the conventional e-log p' space), when considering large variations in confining pressures.[15] This latter effect has been included in a recent model by Crouch *et al.*[16]

2. Most constitutive models for sands are based on the assumption of isotropic material behaviour (using isotropic yield functions[17,18]). However, there is increasing evidence that sands exhibit anisotropic stress–strain properties due to their initial depositional structure[19,20] and subsequent stress history.[10,11,21,22]

In order to achieve reliable predictions of sand behaviour over a wide range of confining pressures and densities, the current formulation introduces the void ratio as an independent state variable. The model uses a single yield function with a series of hardening rules to describe the compression behaviour of freshly deposited sands, variation of peak friction and dilation angles with confining pressure and density, and evolution of anisotropic properties.[9] Pestana and Whittle[23] have established that sand specimens compressed from different initial formation densities approach a unique response at high stress levels, referred to as the limiting compression curve (LCC). Experimental data for shearing of sands at high confining pressures[24,25] show that the critical state and LCC lines are approximately parallel and hence, sands will exhibit normalized behaviour qualitatively similar to the response of resedimented clays. This result provides the basis for unifying the description of clays and sands within a single model formulation. Similar capabilities have been obtained through the use of a hierarchical single surface (HISS) approach and the disturbed state concept (DSC) as proposed by Desai and his coworkers[26–29] for a wide variety of geological materials including rocks.

2. CONSTITUTIVE RELATIONS

The formulation of MIT-S1 is based on the incrementally linearized theory of rate independent elasto-plasticity[30] as summarized in Table I. Incremental strains are decomposed into elastic and plastic components. For simplicity of the formulation, the elastic behaviour is assumed to be isotropic, while plastic strains are obtained from a generalized flow rule. The main conceptual departure from other effective stress models is the explicit inclusion of void ratio as a state variable in the description of the yield function. The following sections describe the main components of the model.

2.1. Compression behaviour

Pestana and Whittle[23] have presented a simple framework for describing hydrostatic compression of 'freshly deposited' cohesionless sands. Sands specimens compressed from different initial formation densities (i.e. at $p' \to 0$; Figure 1) approach a unique limiting compression curve (LCC) at high stress levels, which can be described by a linear relationship in a log e-log p' space, with slope, ρ_c, and reference stress, p'_{ref} at a unit void ratio ($e = 1$, Figure 1). Irrecoverable, plastic strains develop throughout first loading and represent mechanisms ranging from particle sliding and rolling at low stresses to crushing, which is the principal component of deformation for LCC

Table I. Summary of incrementally linearized elastoplasticity as used by the MIT-S1 model

1. Incremental elastoplastic equations

$$\delta\varepsilon = \delta\varepsilon^{e} + \delta\varepsilon^{p}$$

where $\delta\varepsilon$, $\delta\varepsilon^{e}$ and $\delta\varepsilon^{p}$ are the total, elastic and plastic strain increments, respectively. The incremental elastoplastic equations are written as

$$\delta\sigma' = C:\delta\varepsilon^{e} = C:(\delta\varepsilon - \delta\varepsilon^{p})$$

where σ' is the effective stress tensor, C is the elastic stiffness tensor and ' : ' is the double contraction for tensor multiplication. For an isotropic elastic stress tensor, the stress increment can be further decomposed into the volumetric and deviatoric components:

$$\delta\sigma' = \begin{Bmatrix} \delta p' \\ \delta s \end{Bmatrix} = \begin{Bmatrix} K(\delta\varepsilon_{p}^{e}) \\ 2G(\delta\varepsilon_{s}^{e}) \end{Bmatrix} = \begin{Bmatrix} K(\delta\varepsilon_{p} - \delta\varepsilon_{p}^{p}) \\ 2G(\delta\varepsilon_{s} - \delta\varepsilon_{s}^{p}) \end{Bmatrix}$$

where p' is the mean effective stress, $\mathbf{s}$ is the deviatoric stress tensor (i.e. $\sigma' = 1/3\,p'\mathbf{I} + s$), K and G are the current (i.e. tangential) elastic bulk and shear moduli, ε_{p} is the volumetric strain and ε_{s} is the deviatoric strain tensor.

2. Flow rule

$$\delta\varepsilon^{p} = \mathrm{d}\lambda\,\mathbf{P} = \begin{Bmatrix} \delta\varepsilon_{p}^{p} \\ \delta\varepsilon_{s}^{p} \end{Bmatrix} = \mathrm{d}\lambda \begin{Bmatrix} P_{p} \\ P_{s} \end{Bmatrix}$$

where $\mathrm{d}\lambda$ is a scalar parameter defining the magnitude of the plastic strain increment and P defines the direction of the plastic strain increment with volumetric and deviatoric components P_{p} and P_{s}, respectively (i.e. $P = P_{p}\mathbf{I} + P_{s}$)

3. Load direction

$$Q:C:\delta\varepsilon = KQ_{p}\delta\varepsilon_{p} + 2GQ_{s}:\delta\varepsilon_{s} = \begin{cases} \geqslant 0 & \text{Loading} \\ < 0 & \text{Unloading} \end{cases}$$

where Q is the bounding surface gradient tensor with volumetric and deviatoric components, Q_{p} and Q_{s}, respectively ($Q_{p} = \partial f/\partial p'$, $Q_{s} = \partial f/\partial s$), $f(\sigma', e, \alpha', \mathbf{b})$ is the yield function, e is the current void ratio, and α', $\mathbf{b}$ are the internal variables defining the size and orientation of the bounding surface, respectively.

4. Incremental effective stress–strain relationship

$$\begin{Bmatrix} \mathrm{d}p' \\ \delta s \\ \delta e \end{Bmatrix} = \begin{Bmatrix} K(\delta\varepsilon_{p} - \delta\lambda P_{p}) \\ 2G(\delta\varepsilon_{s} - \delta\lambda P_{s}) \\ (1+e)\delta\varepsilon_{p} \end{Bmatrix}, \quad \delta\lambda = \frac{\left(KQ + \dfrac{\partial f}{\partial e}(1+e)\right)\delta\varepsilon_{p} + 2GQ_{s}:\delta\varepsilon_{s}}{H + KQ_{p}P_{p} + 2GQ_{s}:P_{s}}$$

where H is the elasto-plastic modulus, defining hardening of the yield surface.

states. The complete incremental elastoplastic effective stress–strain response of sands in hydrostatic compression is given by

$$\delta\varepsilon_{p} = \frac{e}{1+e}\left[\frac{\delta_{b}^{\theta}}{C_{b}(p'/p_{a})^{1/3}} + \frac{\rho_{c}}{(p'/p_{a})}(1-\delta_{b}^{\theta})\right]\frac{\delta p'}{p_{a}} \tag{1a}$$

$$\delta\varepsilon_{p}^{e} = \frac{e}{1+e}\left[\frac{1}{C_{b}(p'/p_{a})^{1/3}}\right]\frac{\delta p'}{p_{a}} \tag{1b}$$

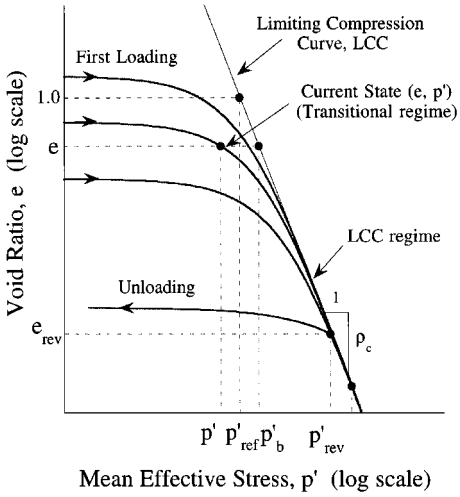

Figure 1. Conceptual model of first loading and unloading of freshly deposited cohesionless soils (after Pestana and Whittle[23])

where $\delta\varepsilon_p$, $\delta\varepsilon_p^e$ are the total and elastic volumetric strain increments, respectively, C_b controls the elastic strains, and P_a is the atmospheric pressure. The parameter θ is a constant exponent ($\theta > 0$) and δ_b is the dimensionless distance between the current mean effective stress and the equivalent LCC mean effective stress, p'_b at the same void ratio (cf. Figure 1):

$$\delta_b = 1 - (p'/p_b), \quad 0 \leqslant \delta_b \leqslant 1 \tag{2a}$$

$$p'_b = p'_{ref}\left(\frac{1}{e}\right)^{1/\rho_c} \tag{2b}$$

Pestana and Whittle[23] show how the three input parameters describing plastic deformation (ρ_c, p'_{ref}, θ) can be readily estimated from hydrostatic or one-dimensional compression tests. They also report selected values for the compression parameters for a wide range of cohesionless soils from which it can be shown that (i) mineralogy has little influence on the LCC parameters; (ii) particle angularity influences all three parameters (ρ_c, p'_{ref}, θ); (iii) mean particle size (D_{50}) affects p'_{ref} and (iv) θ depends on the particle size distribution (and hence, provides a measure of the amount of particle crushing).

The virgin consolidation line of reconstituted clay specimens can also be well characterized by a linear relationship in double logarithmic void ratio-effective stress space[9] and hence, is qualitatively similar to the limiting compression curve. However, mineralogy is the principal factor affecting the slope (ρ_c) of the LCC for reconstituted clays; while the reference stress (p'_{ref}) is related to the grain size distribution (characterized by the clay fraction) and chemical composition of the pore fluid (dielectric constant, concentration of dissolved electrolyte, valence of adsorbed cations and pH).

2.2. Yield and failure conditions

The MIT-S1 model assumes that the strength of soils sheared to large strains can be described by a critical state failure criterion, while the plastic response during shearing is controlled by a separate yield function. Conditions of maximum shear stress (i.e. undrained shear strength) and peak friction angle are controlled by the size, shape and orientation of the yield surface, while large strain (critical state) conditions are considered to be, by and large, independent of previous stress history and density.

Critical state failure conditions are represented by an isotropic function, h_f, of the form proposed by Matsuoka and Nakai,[31] defining a conical surface in effective stress space:

$$h_f(\eta) = k^2 - \eta : \eta = 0 \tag{3a}$$

$$k^2 = k_a^2 + \left(3 - \frac{k_a^2}{2}\right) J_{3\eta}, \quad k_a^2 = \frac{(8 \sin^2 \phi'_{cs})}{(3 + \sin^2 \phi'_{cs})} \tag{3b}$$

where $\eta = s/p'$ is the stress ratio tensor, $\mathbf{s}$ is the deviatoric stress tensor, " : " is the tensor scalar product, and $J_{3\eta}$ is the third invariant of the stress ratio tensor, η:

$$J_{3\eta} = \det|\eta| = \det|\mathbf{s}|/p'^3 \tag{3c}$$

The material constant k (and hence the function h_f) is uniquely defined by the friction angle ϕ'_{cs} measured at large shear strains in triaxial compression tests and is similar in shape to other criteria proposed for soils.[17] The Matsuoka–Nakai criterion has two important properties: (1) the model predicts equal friction angles in triaxial compression and extension modes of shearing (i.e. $\phi'_{csTC} = \phi'_{csTC} = \phi'_{cs}$); and (2) the critical state friction angle is unique for all modes of plane strain shearing. Although there is only mixed experimental support for these assumptions,[20] the Matsuoka–Nakai failure criterion is a good approximation for non-structured materials (i.e. where anisotropic properties arise mainly from consolidation stress history), and provides a continuous differentiable function in stress space.

The shear properties of freshly deposited soils (sands and clays) are characterized by a single yield function whose geometry resembles a distorted lemniscate,[21] and is similar in shape to other surfaces proposed in the literature:[26]

$$f = p'^2[(\eta - b) : (\eta - b) - \zeta^2\left(1 - \left(\frac{p'}{\alpha'}\right)^m\right)] = 0 \tag{4a}$$

$$\zeta^2 = c^2 + b : b - 2\eta : b \tag{4b}$$

where the parameter c controls the aperture of the surface as $p' \to 0$, and m describes the shape (slenderness) of the yield surface.

The size of the yield surface is described by the scalar parameter, α', and its orientation by the second-order anisotropy tensor, b. The model assumes a unique lateral earth pressure coefficient (K_{0NC}) for specimens that are consolidated one dimensionally into the LCC regime, such that the effective stress state is located at the tip of the yield such that $p' = \alpha'$, and $\eta = b$ (i.e. the principal directions of stress and anisotropy coincide). At low confining pressures, the components of the anisotropy tensor are related to the depositional structure of the sand and need not coincide with directions of the applied stresses (although this assumption may be adopted for simplicity).

The parameter c is defined in terms of a (density-dependent) maximum friction angle ϕ'_m occurring in triaxial shear modes and is extended to non-triaxial state conditions using the

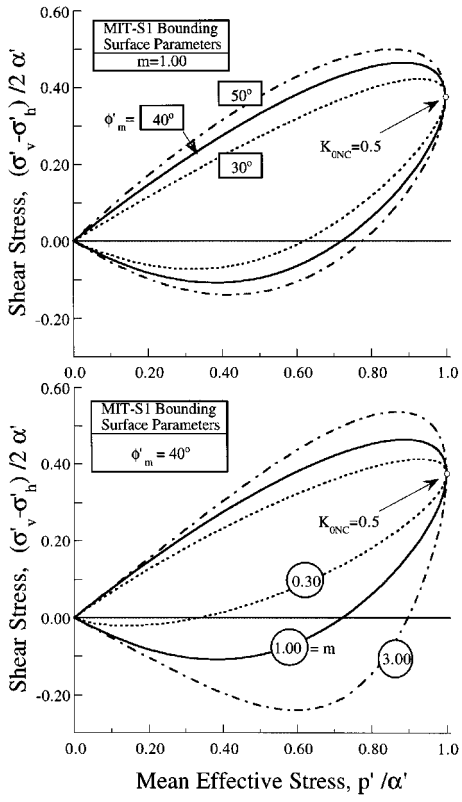

Figure 2. Effect of parameters ϕ'_{m} and m in the shape of the bounding surface

generalization proposed by Matsuoka and Nakai:[31]

$$c^2 = c_a^2 + \left(3 - \frac{c_{\mathrm{a}}^2}{2}\right) \mathrm{J}_{3\eta}, \quad c_{\mathrm{a}}^2 = \frac{(8 \sin^2 \phi'_{\mathrm{m}})}{(3 + \sin^2 \phi'_{\mathrm{m}})} \tag{4c}$$

Figure 2 illustrates how the parameters ϕ'_{m} and m affect the shape of the yield surface K_0-normally consolidated specimens in triaxial space ($K_{0\mathrm{NC}} = 0{\cdot}5$). The proposed yield functional is capable of describing a wide variety of materials[9] ranging from non-plastic silts (with $m \leqslant 0{\cdot}5$) to high plasticity clays ($m \geqslant 3$).

Previous studies[2,32] indicated several important limitations associated with the ellipsoidal-shaped yield surface used by the modified Cam clay (MCC[33]) family of models. Figure 3 compares the yield surface shape of the MCC and MIT-E3 models with the isotropic and anisotropic forms of the proposed yield surface using parameters selected for a sandy clay, Lower Cromer Till,[32,34] with large strain (critical state) friction angles, $\phi'_{\mathrm{csTC}} = \phi'_{\mathrm{csTC}} \approx 30^\circ$. There are large differences in the shapes of the yield surfaces in the supercritical region [i.e. $\eta : \eta > k^2$, equation (3a) in the compression shear mode, and at very high overconsolidation ratio (OCR; i.e. $p'/\alpha' \ll 1$) in all modes of shearing. As the anisotropy increases, the shape of the bounding surface becomes

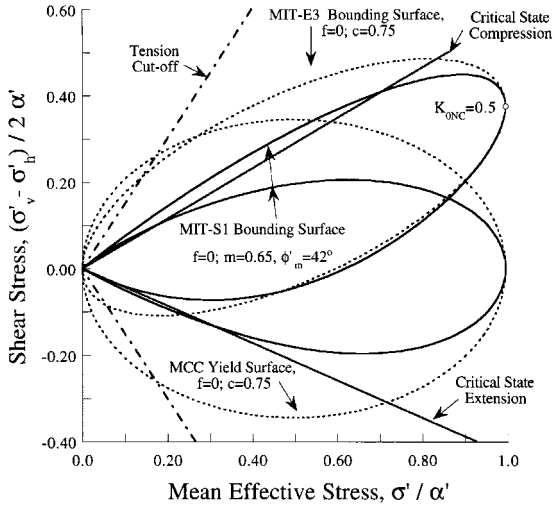

Figure 3. Comparison of isotropic and anisotropic yield functions with MCC isotropic yield surface and MIT-E3 anisotropic bounding surface for lower Cromer Till

more distorted and is controlled by the parameter ζ [cf. equation 4b] which accounts for the effect of current stress ratio, η, and past consolidation history reflected by different states of anisotropy, b. The proposed model restricts the maximum stress ratio, η, through the use of parameter ϕ'_m and hence, eliminates the unrealistic values of stress obliquity predicted by both the MCC and MIT-E3 models.

For sands, the peak friction angles in drained shearing are functions of the current density[35,36] as well as confining stress.[37] In many existing elasto-plastic constitutive models, this behaviour is simulated by adjusting the input parameters controlling the shape of the yield surface for each density (and confining pressure) of interest.[17,18,28] For cohesive soils, there is much less experimental evidence linking the peak friction angle to the current density, and most constitutive models assume that shape of the yield surface is unique (e.g. MCC), leading to normalized stress–strain–strength properties. The new model assumes that changes in shape of the yield surface with density can be related primarily to the aperture of the circumscribing cone. Hence, the parameter m is treated as a material constant, while the aperture hardening is controlled by parameter ϕ'_m defined as a function of current void ratio, e:

$$\operatorname{cotan} \phi'_m = \operatorname{cotan}(45^\circ + \phi'_{cs}/2) + [\operatorname{cotan} \phi'_{mr} - \operatorname{cotan}(45^\circ + \phi'_{cs}/2)](e)^p \tag{5}$$

where ϕ'_{mr} is the reference value of the maximum friction angle at a unit void ratio ($e = 1$), and p is a material constant that describes the change of ϕ'_m with density as shown in Figure 4. As the void ratio decreases ($e \to 0$), the friction angle ϕ'_m in triaxial compression (and extension) predicted by equation (5) approaches a maximum value of $\phi'_m(e \to 0) = [45^\circ + \phi'_{cs}/2]$ which provides an upper bound to parameter ϕ'_m. The peak friction angle becomes independent of the void ratio when $p = 0$ (i.e. $\phi'_m = \phi'_{mr}$), corresponding to the normalized behaviour of normally and lightly over consolidated clays.

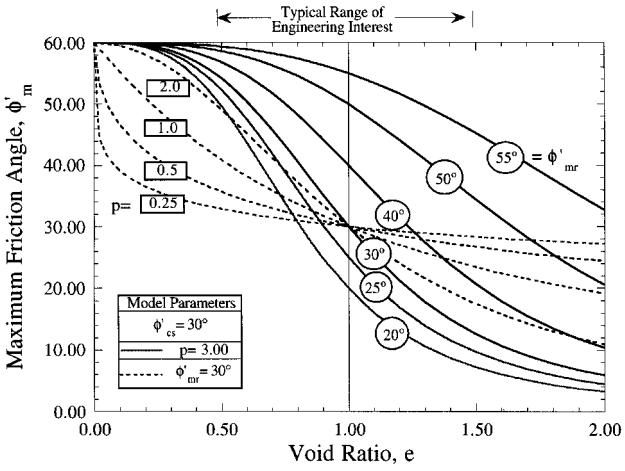

Figure 4. Effect of current density on yield surface geometry

2.3. *Hardening and flow rules*

The model uses two hardening laws that describe changes in the size and orientation of the yield surface in order to represent: (1) the normalized behaviour of sands and clays in the LCC regime; and (2) the transition from dilative to contractive behaviour as a function of confining pressure (non-normalizable behaviour). The load direction for stress states with $f = 0$ (i.e. 'plastic states'), is given by the yield function gradient, Q:

$$Q = \frac{\partial f}{\partial \sigma'} = \begin{Bmatrix} \partial f/\partial p' \\ \partial f/\partial s \end{Bmatrix} = \begin{Bmatrix} Q_{\mathrm{p}} \\ Q_{\mathrm{s}} \end{Bmatrix} \tag{6a}$$

$$Q_{\mathrm{p}} = p'\left[(m\zeta^2 + 2\eta : b)\left(\frac{p'}{\alpha'}\right)^{\mathrm{m}} - 2\eta : \eta + \left(9 - \frac{3c_{\mathrm{a}}^2}{2}\right)\left(1 - \left(\frac{p'}{\alpha'}\right)^{\mathrm{m}}\right)\mathrm{J}_{3\eta}\right] \tag{6b}$$

$$Q_{\mathrm{s}} = p'\left[2\left(\eta - \left(\frac{p'}{\alpha'}\right)^{\mathrm{m}} b\right) - \left(3 - \frac{c_{\mathrm{a}}^2}{2}\right)\left(1 - \left(\frac{p'}{\alpha'}\right)^{\mathrm{m}}\right)\frac{\partial \mathrm{J}_{3\eta}}{\partial \eta}\right] \tag{6c}$$

where Q_{p}, Q_{s} are the volumetric and deviatoric components of the yield surface gradient tensor, Q. The last term in expressions (6b) and (6c) represents the contribution of the Matsuoka generalization of the yield surface, and adds significant algebraic difficulty in the derivation of the yield surface gradient tensor compared with previous derivations.

Kinematic hardening of the bounding surface is based on the concept that the principal directions of anisotropy, in general, rotate towards the principal stress axes;[39]

$$\delta b = \psi \frac{(1+e)}{e\alpha'}\left\{\frac{r_x}{m}\langle Q_{\mathrm{p}}\delta\varepsilon_{\mathrm{p}}^{\mathrm{p}}\rangle + r_y|Q_{\mathrm{s}} : \delta\varepsilon_{\mathrm{s}}^{\mathrm{p}}|\right\}(\eta - b) \tag{7}$$

where ψ is dimensionless material constant controlling the rate of change in anisotropy, and $\langle\ \rangle$ are the Macaulay brackets. The kinematic hardening for this model depends on the deviatoric

plastic strain increments $\delta\varepsilon_s^p$, as well as the volumetric strains, $\delta\varepsilon_s^p$. The parameters $r_x(\eta, \phi'_{cs})$ and $r_y(\eta, K_{0NC})$ impose limits on the principal directions of anisotropy for consolidation along radial effective stress paths and the 'residual anisotropy' for shearing to large strain (critical state) conditions, respectively:

$$r_x = (k^2 + b:b - 2\eta:b)/k_a^2 \tag{8a}$$

$$r_y = (d^2 + b:b - 2\eta:b)\left(1 + \left(\frac{\alpha'}{p'} - 1\right)\delta_b^\theta\right) \tag{8b}$$

where the scalar parameter 'd' follows from a Matsuoka-type generalization and is related to the lateral stress ratio at rest for 'normally consolidated' materials in the LCC regime, K_{0NC}:

$$d^2 = d_a^2 + (3 - d_a^2/2)\mathrm{J}_{3\eta}, \quad \mathrm{d}_a^2 = \frac{2(1 - K_{0NC})^2}{(1 + K_{0NC} + K_{0NC}^2)} \tag{8c}$$

For consolidation along radial stress paths (i.e. $\eta = \mathbf{b}$, $\mathbf{Q}_s = 0$) the scalar parameter r_x in equation (8a) predicts full reorientation of the yield surface with directions of anisotropy limited by the critical state failure condition (i.e. $\mathbf{b}:\mathbf{b} \leqslant k^2$). For K_0-normally consolidated specimens, the parameter r_x ensures that directions of anisotropy evolve more slowly when shearing in a compression mode than in a similar extension test.

For one-dimensional consolidation, the scalar r_y [equation 8b] guarantees full reorientation of the yield surface to the prescribed value of K_{0NC} while controlling the residual anisotropy at critical state conditions ($\delta\varepsilon_p^p = 0$). The model predicts increased softening for samples consolidated at increasing shear stress levels when sheared in the same direction of the consolidation shear stress, as observed exprimentally.[34,40,41] The parameter r_y also allows the yield surface of specimens initially consolidated at high stress obliquity, to undergo a net reduction in anisotropy (reduction in b) when sheared to the critical state (residual) condition.[42]

Changes in the size of the yield surface are related to both the plastic volumetric and share strains ($\delta\varepsilon_p^p$, $\delta\varepsilon_s^p$), similar in concept to other sand models:[43]

$$\frac{\delta\alpha'}{\alpha'} = \frac{(1 + e)}{e(\rho_c - \rho_r)(1 - \delta_p^\theta)}\left[\delta\varepsilon_p^p + \delta_p^\theta\left(\frac{Q_s:\delta\varepsilon_s^p}{p'}\right)\right] - \frac{2b:\delta b}{(a^2 + b:b)} \tag{9}$$

where $a(\phi'_{cs})$ is a constant controlling the spacing of the limiting compression curves for soils consolidated along radial effective stress paths (with $\eta = \text{const}$); δ_p is the normalized distance of the current yield surface to the hydrostatic limiting compression curve (H-LCC) generalizing the compressibility of sands to non-hydrostatic stress conditions:

$$\delta_p = 1 - \frac{\alpha'}{p'_b}\left(1 + \frac{b:b}{a^2}\right), \quad 0 \leqslant \delta_p \leqslant 1 \tag{10a}$$

$$a^2 = 24\sin^2\phi'_{cs}/(3 - \sin\phi'_{cs})^2 \leqslant 1 \tag{10b}$$

For soils in the LCC regime (including all K_0-normally consolidated clays), $\delta_p = 0$, and equations (9) and (10) can be simplified to give:

$$\frac{\delta\alpha'}{\alpha'} = \frac{(1 + e)}{e(\rho_c - p_r)}\delta\varepsilon_p^p - \frac{2b:\delta b}{(a^2 + b:b)} \tag{11}$$

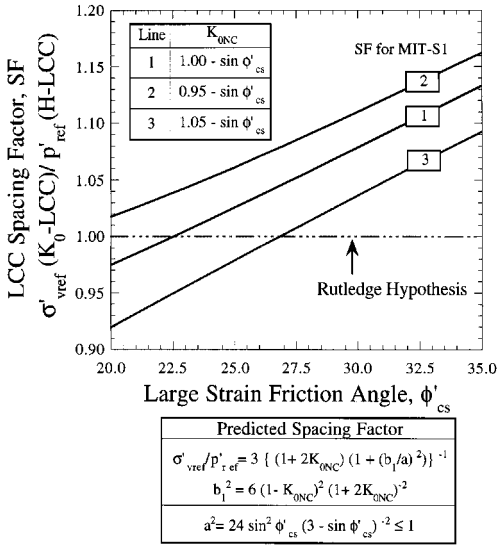

Figure 5. Relative location of K_0 and hydrostatic limiting compression curves

The proposed formulation guarantees the robustness of the Limiting compression curves (LCC) for radial effective stress paths[34] and is presented in detail in Appendix II. As result, the location of the LCC lines for radial consolidation (i.e. constant stress ratio) is independent of the rate of yield surface rotation, in contrast with previous formulations.[9]

Figure 5 shows the predicted spacing of the limiting compression curves in one-dimensional and hydrostatic compression, denoted by the ratio of the reference major principal stress $\mathrm{SF} = \sigma'_{\mathrm{vref}}/p'_{\mathrm{ref}}$ as a function of the critical state friction angle, ϕ'_{cs} and $K_{0\mathrm{NC}}$ and compares it to the Rutledge hypothesis which state that volume changes during radial consolidation are only a function of the major principal stress,[44] σ'_1. Although in principle, it is possible to select the parameter 'a' [equation (10b)] from the measured spacing of the K_0-LCC and the H-LCC, lines, this data is seldom available. Pestana and Whittle[32] show that use of expression (10b) gives excellent prediction of the location of the H-LCC for K_0-consolidated specimens of Lower Cromer Till which are swelled to a hydrostatic stress condition and re-consolidated hydrostatically. Coop[45] reports K_0 and hydrostatic compression for calcareous Dog's Bay sand which suggests that the Rutledge hypothesis is a good approximation (i.e. $\sigma'_{\mathrm{vref}}/p'_{\mathrm{ref}} = 1{\cdot}00 \pm 0{\cdot}05$), while Figure 5 predicts $\sigma'_{\mathrm{vref}}/p'_{\mathrm{ref}} \approx 1{\cdot}09$ (for $K_{0\mathrm{NC}} = 0{\cdot}50$, $\phi'_{\mathrm{cs}} = 40^\circ$). For typical values of critical state friction angles (cf. Figure 5), the proposed formulation predicts spacing ratio values within 5–10% of those obtained from the Rutledge hypothesis.

The functional form in equation (11) states that changes in the size of the yield surface for sands are decoupled from changes in void ratio (or plastic volumetric strains) in the transitional regime ($\delta_{\mathrm{p}} \neq 0$) and are a function of both plastic volumetric, $\delta\varepsilon^{\mathrm{p}}_{\mathrm{p}}$, and plastic shear strains, $\delta\varepsilon^{\mathrm{p}}_{\mathrm{s}}$, a concept first introduced by Nova and Wood.[43] However, in contrast to previous formulations, the change in size of the surface is neither related to critical (or steady)-state conditions,[14,16] nor unbounded,[17,43,46] but is controlled by the limiting compression curve, LCC. For soils in the LCC

regime ($\delta_p = 0$) hardening in the size of the yield surface is related, primarily to changes in void ratio, thus converging to the normalized behaviour of clays.

Plastic strains on the yield surface are described by a non-associated flow rule which satisfies two basic constraints: (1) shearing at the critical state causes no further change in volume; and (2) one-dimensional consolidation of normally consolidated soils in the LCC regime is characterized by the measured stress ratio, K_{0NC}. The directions of plastic flow are controlled by a second-order tensor, **P**, with volumetric and deviatoric components (P_p, P_s, respectively), defined as follows:

$$P_p = \begin{cases} (k^2 - \eta : \eta)\dfrac{p'}{\alpha'}(1 - \delta_p)^m & \text{Subcritical region, } \eta : \eta \leqslant k^2 \\ (k^2 - \eta : \eta)\dfrac{p'}{\alpha'} & \text{Supercritical region, } \eta : \eta \geqslant k^2 \end{cases} \tag{12a}$$

$$P_s = xP_p\eta + \frac{\zeta^2|\eta|}{\alpha'}Q_s \tag{12b}$$

where the parameter x is defined in terms of K_{0NC}.[1]

$$x = \left(\frac{\rho_c}{\rho_c - \rho_r}\right)\left\{\frac{1}{3}\left(\frac{1 - 2K_{0NC}}{1 - K_{0NC}}\right) - \frac{K}{2G}\left(\frac{\rho_r}{\rho_c}\right)\right\}. \tag{13}$$

The plastic formulation is completed by invoking the consistency requirement that the stress state remains in contact with the yield surface (i.e. $df[\sigma', e, \alpha, \mathbf{b}] = 0$), from which the elasto-plastic modulus, H can be derived:

$$\delta\lambda H = -\frac{\partial f}{\partial \alpha'}\delta\alpha' - \frac{\partial f}{\partial b} : \delta b \tag{14a}$$

$$\delta\lambda = \frac{\left[KQ_p + \dfrac{\partial f}{\partial e}(1 + e)\right]\delta\varepsilon_p + 2GQ_s : \delta\varepsilon_s}{H + KQ_pP_p + 2GQ_s : P_s} \tag{14b}$$

where K and G are the elastic bulk and shear moduli as defined in the next section, $\partial f/\partial e$ represents the change in the shape of the yield surface with respect to void ratio, and $\delta\lambda$ is a scalar controlling the magnitude of the plastic strain increment (cf. Table 1)

2.4. *Hysteretic and bounding surface formulations*

The proposed model represents the unloading and reloading behaviour through two components: (1) equations to describe the non-linear but reversible response during unloading and reloading at constant stress ratio, η, or constant mean effective stress, p', referred to as 'perfectly hysteretic' response;[47] and (2) development of irrecoverable (plastic) strains for stress paths approaching the yield surface through a bounding surface formulation.[48] Figure 6 illustrates the modelled representation of unloading and reloading in a one-dimensional compression test (marked O-A-B). In this example, the soil specimen is initially consolidated to a state (O) in the LCC regime. The stiffness at load reversal is controlled by the small strain isotropic elastic stiffness parameters K_{max}, G_{max}. The subsequent non-linear swelling response is related to the stress state at last reversal (i.e. point O). On reloading from A, the initial stiffness is again governed by the small strain elastic stiffness, while the additional bounding surface plastic strains

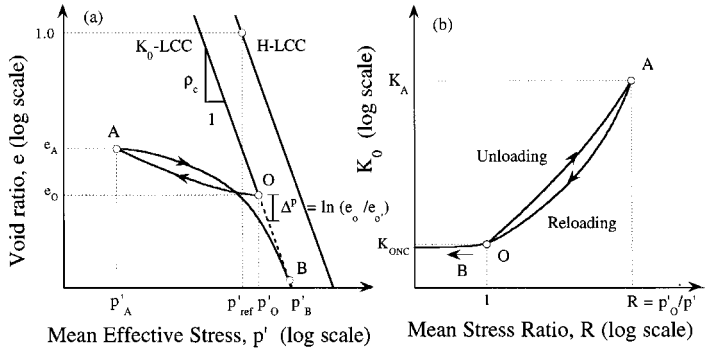

Figure 6. Conceptual model of first load and unload–reload for hydrostatic and 1-D compression

introduce irrecoverable strains (cf., Figure 6) and path-dependent behaviour (witnessed by differences in the lateral stressed ratio K_0).

2.4.1. Hysteretic equations. The proposed model does not have a region of true elastic behaviour. The response immediately after a load reversal is controlled by the small strain elastic moduli ($K_{\max}$, $G_{\max}$) given by:

$$\frac{K_{\max}}{p_a} = C_b \left(\frac{1+e}{e}\right)\left(\frac{p'}{p_a}\right)^{1/3}\left(1 + \left(\frac{K_{\max}}{2G_{\max}}\right)\eta : \eta\right)^{1/6} \tag{15a}$$

$$\frac{2G_{\max}}{K_{\max}} = 3\left(\frac{1-2\mu'_0}{1+\mu'_0}\right) \tag{15b}$$

where C_b is a dimensionless material constant, and μ'_0 is the small strain Poisson's ratio observed immediately after a load reversal. Equations (15a) and (15b) provide an incrementally conservative elastic formulation[49] and are similar to those proposed previously for sands[50,51] but they are written in terms of the tangent moduli and explicitly include the effect of the current void ratio, e, in the soil stiffness.

Pestana and Whittle[23] discuss the different methods for estimating the parameter C_b, using: (1) direct measurements of volumetric strain in hydrostatic unloading tests; (2) vertical strain measurements in one-dimensional swelling tests (using rigid-walled oedometer or triaxial test equipment); or (3) indirect interpretation from laboratory measurements of the small strain elastic shear modulus, $G_{\max}$ (e.g. resonant column, piezo-electric transducers, etc). The small strain elastic Poisson's ratio, μ'_0 can be estimated from the effective stress path measured during one-dimensional swelling in a laboratory triaxial apparatus ($\Delta\varepsilon_v < 0$, $\Delta\varepsilon_h = 0$):

$$\mu'_0 = \frac{\Delta\sigma'_h/\Delta\sigma'_v}{1 + \Delta\sigma'_h/\Delta\sigma'_v} \tag{15c}$$

where $\Delta\sigma'_h/\Delta\sigma'_v$ is the slope of the observed effective stress path immediately after load reversal. However, these measurements require high-quality control of lateral strains during swelling.

The non-linear hysteretic response is modelled by relating the isotropic tangent moduli to the most recent stress reversal state. The formulation includes a variable Poisson's ratio to describe

more realistically the variation of $K_0(=\sigma'_h/\sigma'_v)$ measured during one-dimensional swelling and subsequent reloading (cf. Figure 6):

$$\left(\frac{2G/K}{2G_{max}/K_{max}}\right)=\begin{cases}\dfrac{1}{(1+\omega\xi_s)} & \text{for unloading, } p'<p'_{rev}\\ \dfrac{1}{(1+\omega\xi\xi_s)} & \text{for reloading, } p'\geqslant p'_{rev}\end{cases} \tag{16}$$

where ω is a constant (estimated from the effective stress path in one-dimensional swelling from an initial LCC state), and ξ and ξ_s are dimensionless stress measures defined as follows:

$$\xi=\begin{cases}p'/p'_{rev} & \text{for } p'<p'_{rev}\\ p'_{rev}/p' & \text{for } p'\geqslant p'_{rev}\end{cases},\quad \xi\leqslant 1 \tag{17a}$$

$$\xi_s=\{(\eta-\eta_{rev}):(\eta-\eta_{rev})\}^{1/2},\quad \eta=\mathbf{s}/p' \tag{17b}$$

where p'_{rev} and η_{rev} are the mean effective stress and the stress ratio tensor at the stress reversal point.

Equation (16) describes a variable Poisson's ratio during unloading which is bounded in the range $\mu'_0\leqslant\mu'<0{\cdot}50$. The equivalent Poisson's ratio, μ', for shearing at constant mean effective stress can be expressed as a function of the stress reversal distance in deviatoric space, ξ_s:

$$\mu=\frac{\mu'_0+\frac{1}{3}\omega\xi_s(1+\mu'_0)}{1+\frac{2}{3}\omega\xi_s(1+\mu'_0)},\quad \mu'_0\leqslant\mu'<0{\cdot}50 \tag{18}$$

Figure 7 illustrates the effect of the parameters μ'_0 and ω on the effective stress paths for one-dimensional swelling (from an initial consolidation stress state σ'_{vc}, and $K_{0NC}=0{\cdot}49$). In contrast to previous models,[1,17] unloading along a linear strain path (i.e. constant ratio of applied strain increments) does not generate a linear effective stress path. The figure also includes typical laboratory data, which show the similarity in swelling behaviour of an uncemented Pennsylvania sand and Boston Blue clay. Non-linearity of the effective stress paths for these two soils is apparent at $\sigma'_v/\sigma'_{vc}\leqslant 0{\cdot}5$ (OCR $\geqslant 2$) and can be well described by equation (16), with $\omega=1$.

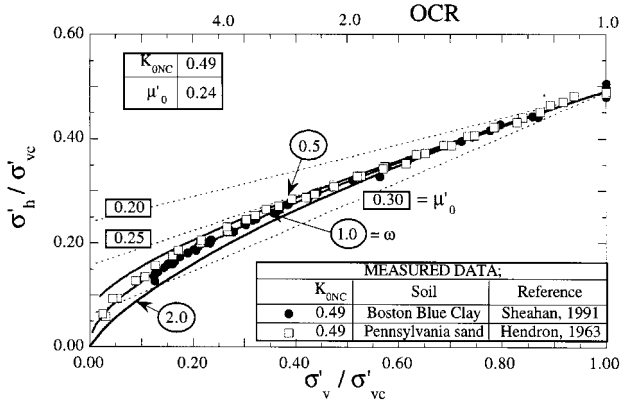

Figure 7. Evaluation of input parameters μ'_0 and ω from effective stress paths in one-dimensional swelling

The tangent bulk modulus during unloading is described by the following expression:

$$\frac{K}{p_a} = \frac{(1+e)}{e\rho_r}\frac{p'}{p_a} \tag{19a}$$

$$\rho_r = D(1-\xi^r) + \frac{(1+\omega_s\xi_s)}{C_b\left(1+\left(\frac{K_{max}}{2G_{max}}\right)\eta:\eta\right)^{1/6}}\left(\frac{p'}{p_a}\right)^{2/3} \tag{19b}$$

where ρ_r is the current (tangential) slope of the swelling curve in a $\log e$–$\log p'$ space diagram, constant and r describe the non-linear behaviour measured during hydrostatic or one-dimensional swelling; and ω_s represents the (small strain) non-linearity during undrained shearing.

For clays, the (one-dimensional or hydrostatic) swelling response can be normalized with respect to stress states on the Limiting Compression Curve (i.e. swelling lines are nearly parallel in the $\log e$–$\log p'$ space). The incremental elastic strains arising from the second term in equation (19b) are negligible as $p' \to 0$ and hence, the swelling behaviour is controlled by D, r and the current stress reversal ratio, ξ, as shown in Figure 8. The parameter D describes the tangent swelling stiffness at stress reversal ratio $\xi \approx 0{\cdot}1$–$0{\cdot}2$, while r can be estimated by curve fitting the measured volumetric behaviour at intermediate overconsolidation ratios (in the range $0{\cdot}2 \leqslant \xi < 1{\cdot}0$). For sands, volumetric hysteresis at constant stress ratio is negligible (i.e. $D \approx 0$, hence r is not needed) and the hydrostatic or one-dimensional swelling behaviour can be described by C_b only.

Non-linearity for shearing at small shear strain levels is described by the tangent shear stiffness, G, in equations (16) and (19). Re-arrangement of these equations reveals the degradation of elastic shear modulus, G, for shearing at constant mean effective stress (approximating the undrained shearing of overconsolidated soils, $\xi = 1$):

$$\frac{G}{G_{max}} = \frac{1}{(1+\omega\xi_s)(1+\omega_s\xi_s)} \tag{20}$$

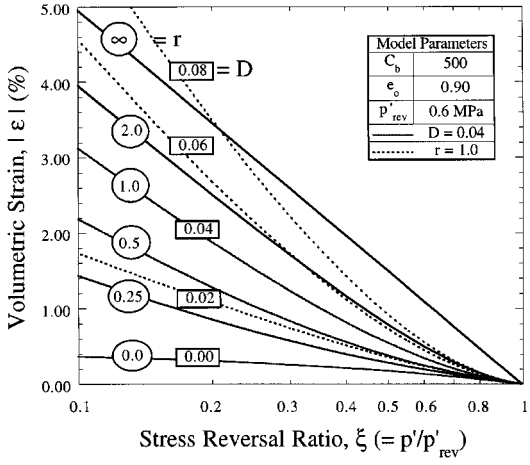

Figure 8. Evaluation of input parameters D and r from the volumetric response during hydrostatic unloading

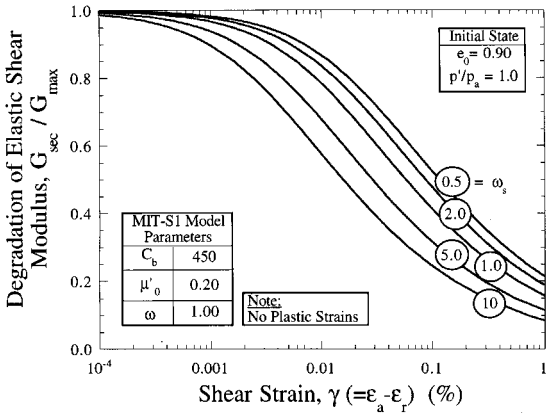

Figure 9. Effects of input parameter ω_s in the shear modulus degradation in undrained triaxial tests

where G is the tangent modulus at the current stress level and G_{max} is the maximum modulus immediately after load reversal.

The parameter ω_s can then be determined from accurate measurement of the shear stress–strain curves. Figure 9 shows the effect of parameter ω_s on the shear modulus degradation (plotted in terms of the secant shear modulus, G_{sec}/G_{max}). The proposed model predicts a response that is qualitatively very similar to experimental data published for both sands[52] and clays.[53]

The model introduces a scalar strain amplitude parameter, χ, in order to define the stress reversal point (SRP) as follows:

$$\chi\dot{\chi} = \begin{Bmatrix} {}^{\Delta 1}\varepsilon_p \delta\varepsilon_p & \text{for } \delta\varepsilon_p \neq 0 \\ {}^{\Delta 1}\varepsilon_s : \delta\varepsilon_s & \text{for } \delta\varepsilon_p = 0 \end{Bmatrix} = \begin{cases} > 0 & \text{loading} \\ \leqslant 0 & \text{unloading (SRP)} \end{cases} \tag{21}$$

where ${}^{\Delta 1}\varepsilon$ is the accumulated strain relative to the previous stress reversal state, and can be decomposed into its volumetric and deviatoric components ${}^{\Delta 1}\varepsilon_p (= \varepsilon_p - \varepsilon_{prev})$, ${}^{\Delta 1}\varepsilon_s (= \varepsilon_s - \varepsilon_{srev})$. It should be noted that separate loading definitions are used for hysteretic and plastic components of the current model.

2.4.2. Bounding surface plasticity. The proposed model uses the concepts of bounding surface plasticity[48] in order to define plastic strains for overconsolidated materials based on the formulation already presented for freshly deposited sands and normally consolidated clays. The yield function [equation 4] acts as the bounding surface, while the plastic strains of the overconsolidated soil are linked to the behaviour at a unique image point on this surface through a radial mapping rule with a homothetic (i.e. same shape) loading surface as shown in Figure 10. The occurrence of plastic strains for the overconsolidated soil is contingent on the loading condition:

$$KQ_p^I \delta\varepsilon_p + 2G(Q_s^I : \delta\varepsilon_s) \quad \begin{cases} \geqslant 0 & \text{loading} \\ < 0 & \text{unloading} \end{cases} \tag{22}$$

where Q^I is the gradient of the bounding surface at the image point (with volumetric and deviatoric components, Q_p^I, Q_s^I, respectively). Hardening of the bounding surface for loading at

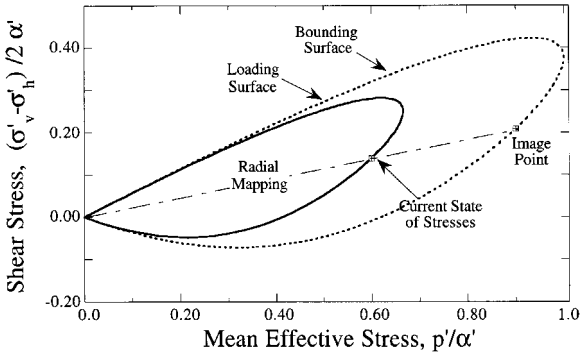

Figure 10. Definition of image point and loading surface for bounding surface plasticity formulation for MIT-S1 model

current stress state is assumed to occur as if the stress state were located at its image point (cf. Figure 10). This implies that the behaviour at the normally consolidated image stress (equivalent pressure) acts as limit or the behaviour of the overconsolidated soil.

For stress states within the bounding surface, plastic strains are defined by specifying the elasto-plastic modulus, H, and flow direction, $\mathbf{P}$, for loading at the current stress state. Separate mapping rules are used for the elasto-plastic modulus and flow direction:

$$\mathbf{P} = \mathbf{P}^{\mathbf{I}}(1 - g_1) + \mathbf{P}^0 g_1 \tag{23a}$$

$$H = \langle H^{\mathrm{I}} \rangle + H^0 \frac{g_1}{1 - g_1} \left(1 - \frac{\eta : \eta}{c^2}\right)^{1/2} \tag{23b}$$

where $\mathbf{P}^0$ and $\mathbf{P}^{\mathbf{I}}$ are the values of $\mathbf{P}$ at first yield and at the image point, respectively; H^0 defines the transition to the LCC; $\langle\ \rangle$ are the Macaulay brackets and g_1 is a mapping function describing the relative position of the current stress and image stress states:

$$g_1 = \frac{\alpha' - \alpha'_0}{\alpha' - \alpha'_{0\mathrm{i}}}, \quad 0 \leqslant g_1 \leqslant 1 \tag{24}$$

where α' is the size of the bounding surface and α'_0, $\alpha'_{0\mathrm{i}}$ are the sizes of the current load surface and the load surface at first yield, respectively. The mapping function g_1 describes two important observations of soil behaviour: (1) At first yielding, $\alpha'_0 = \alpha'_{0\mathrm{i}}$ and $H \to \infty$ so that there is a smooth matching of the perfectly hysteretic and bounding surface models; and (2) As the stress state approaches the bounding surface, $\alpha'_0 \to \alpha'$, both H and $\mathbf{P}$ tend to the value at the image point, and hence describe a smooth transition in behaviour to that of the normally consolidated state. The selection of functions to represent $\mathbf{P}^0$ and H^0 is based on experimental observations of unload–reload behaviour of soils in hydrostatic compression and undrained shearing:

$$P^0_{\mathrm{p}} = -2|\eta - \mathbf{b}| \left|\frac{\mathbf{s}}{\alpha'}\right|, \quad \mathbf{P}^0_{\mathrm{s}} = \mathbf{P}^{\mathbf{I}}_{\mathrm{s}} \tag{25a}$$

$$H_0 = \left(\frac{\rho_{\mathrm{r}}}{\rho_{\mathrm{c}} - \rho_{\mathrm{r}}}\right) \frac{h}{(1 - \delta^{\theta}_{\mathrm{p}})} K^{\mathbf{I}}_{\max} |\mathbf{Q}^{\mathbf{I}}| \, |\mathbf{P}^{\mathbf{I}}| \tag{25b}$$

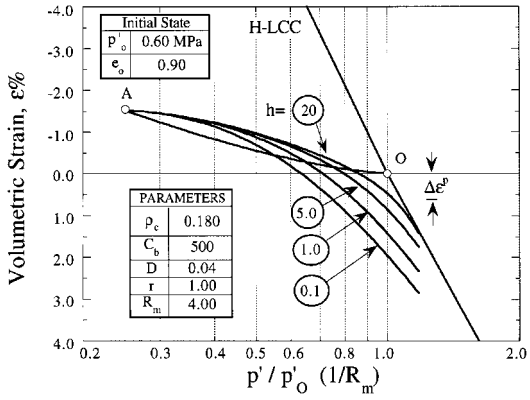

Figure 11. Evaluation of parameter h from the residual plastic strain during reloading

where h is a dimensionless material constant, and K^{I}_{max} is the elastic bulk modulus at the image point. Unfortunately, it is very difficult to ascribe physical meaning to the bounding surface mapping rules. However, the input parameter h can be estimated conveniently by measuring the residual plastic strain accumulated after one or more cycles of loading. For example, Figure 11 shows the effect of h on model predictions of hydrostatic reloading of a clay. For an unload–reload cycle of magnitude R_m, there is a marked increase in the residual plastic strains, $\Delta\varepsilon^p$, as h decreases. Similarly, the residual plastic strain $\Delta\varepsilon_p$ increases with R_m for a selected value of h, as expected from experimental data.

The compressibility of sands at low confining pressures (i.e. in the transitional regime) is small and therefore, it is very difficult to measure residual strains for a single unload–reload cycle. Instead, a better approach for calibrating h is to measure the accumulation of strains of (undrained) shear-induced pore pressures over several load cycles.

3. EVALUATION OF INPUT PARAMETERS

This section summarizes the selection of input parameters used by the model for freshly deposited sands and clays which are resedimented from a slurry condition. Table II gives a complete list of input parameters used by the MIT-S1 mode. Only 13 input parameters are required in order to characterize clays, while 14 input parameters are used for freshly deposited sands. Although the model formulation is relatively complex, all of the input parameters for these materials can be selected from standard types of laboratory test as follows:

1. The parameters ρ_c, p'_{ref} and θ characterize the compression behaviour of freshly deposited sands and can be interpreted from one-dimensional compression tests where specimens are loaded to high confining pressures (typically $p'/p_a \geqslant 100$). Typical ranges of these parameters ($\rho_c = 0{\cdot}37$–$0{\cdot}43$; $p'_{ref} = 3{\cdot}0$–$12{\cdot}0$ MPa, $\theta = 0{\cdot}15$–$0{\cdot}70$) have been proposed by Pestana and Whittle[23] based on published data for more than 20 different sands. The virgin consolidation line of resedimented clay corresponds to the LCC regime, and can be characterized by the compressibility parameter, ρ_c only. Pestana[9] reports $\rho_c = 0{\cdot}14$–$0{\cdot}60$ for a wide range of clays, while normal insensitive clays exhibit $\rho_c = 0{\cdot}25 \pm 0{\cdot}10$.

Table II. Summary of MIT-S1 model input parameters

Parameter	Physical meaning	Suggested method of estimation: sands	Suggested method of estimation: clay
ρ_c	Compressibility of sand in the LCC regime (VCL for sedimented clay)	High stress triaxial or oedometer measurements required	Obtain from standard compressibility index of NC clay (C_c)
p'_{ref}	Reference stress (Figure 1) — defines LCC at void ratio, $e = 1$	High stress triaxial or oedometer measurements required	Not needed for sedimented clays which exhibit normalized behavior
θ	Transitional compression behaviour	1 − D or hydrostatic compression curve to high-pressure range (i.e. LCC regime)	Not needed for resedimented clays
D r	Non-linear volumetric swelling and volumetric hysteresis response	Not needed for sands as volumetric hysteresis is small	Measure 1-D swelling curve (Fig. 8)
h	Irrecoverable plastic strain for unload–reload cycle	Calibrate from accumulated plastic strain in multiple unload–reload cycles	Calibrate from 1-D reload curve (Fig. 11)
K_{0NC}	Lateral earth pressure ratio in the LCC regime	Measure in high-pressure LCC range in automated triaxial tests	Measure for NC clays following SHANSEP consolidation
C_b	Small strain elastic compressibility (at load reversal)	Derive from elastic wave velocity measurements [$\rightarrow G_{max}$; Equations (15a, b)]	
μ'_0	Poisson's ratio at load reversal	Measure effective stress path during 1-D swelling from LCC state (to OCR $\approx$ 5–10) (Figure 7)	
ω	Non-linearity in Poisson's ratio	Measure effective stress path during 1-D swelling from LCC state (to OCR $\approx$ 5–10) (Figure 7)	
ϕ'_{cs}	Large strain (critical state) friction angle	Measure in undrained triaxial compression shear tests (-dense sand)	Measure in undrained triaxial compression shear tests
ϕ'_m or ϕ'_{mr}	Apex angle of bounding surface	Measure peak friction angle in drained triaxial shear tests at two densities (Figure 4)	Undrained strength ratios in triaxial compression and extension tests at OCR = 1
p	Transition from contractive to dilative behaviour	Measure peak friction angle in drained triaxial shear tests at two densities (Figure 4)	Not needed ($p = 0$)
m	Shape of bounding surface	Measure effective stress paths in undrained triaxial compression (— dense sand)	Shape of effective stress paths in CK_0UC, CK_0UE tests at OCR = 1
ω_s	Small strain non-linearity in shear	Local measurement of small strain ($0{\cdot}001 \leqslant \gamma \leqslant 0{\cdot}1$ percent) shear stiffness or modulus degradation (cf. Figure 9)	
ψ	Rate of evolution of anisotropy due to stress history	Measure undrained stress–strain response for dense sand at moderate to large shear strains ($5 \leqslant \gamma \leqslant 20$ percent)	Measure undrained stress–strain behaviour in undrained shear (CK_0UE and/or CK_0UC) at moderate to large shear strains ($5 \leqslant \gamma \leqslant 20$ per cent)

2. The parameters D and r describe non-linearity in the volumetric response, and are only required for clays ($D = 0$ is assumed for sands). The parameters can be estimated by matching computed one dimensional swelling strains (cf. Figure 9) with laboratory data from conventional oedometer or constant rate of strain (CRS) consolidation tests.
3. The parameter h is only required when using the model to predict the behaviour of mechanically overconsolidated soils. For clays, h can be estimated from measurements of residual plastic strain overconsolidated soils. For clays, h can be estimated from measurements of residual plastic strain $\Delta\varepsilon^{p}$ (Figure 11) in one-dimensional consolidation tests (CRS or oedometer) tests, preferably using at least two different magnitudes of unload–reload cycle. For sands, the residual plastic strains in a single cycled are very small, and h is more easily calibrated from the residual strain accumulated over a series of unload–reload cycles.
4. The model assumes a constant coefficient of lateral earth pressure for one-dimensional consolidation in the LCC regime, K_{0NC}. This parameter can be measured directly from one-dimensional consolidation tests performed in a (high pressure) automated triaxial cell[56] or lateral pressure measurements in a rigid-walled oedometer[57] tests. Alternatively, it can be estimated from empirical formulae.[58,59]
5. The parameters μ'_0 and ω describe the Poisson's ratio immediately after load reversal, and the variation of the elastic Poisson's ratio accompanying changes in stress ratio, respectively [equation (15) and (18)]. Both parameters can be determined from the effective stress path measured during one dimensional swelling in automated (high-pressure) triaxial tests. Jamiolkowski *et al.*[60] report $\mu'_0 = 0{\cdot}20$–$0{\cdot}25$ for uncemented cohesionless soils, while Pestana[9] reports $\omega = 1{\cdot}0 \pm 0{\cdot}5$ for both sands and clays.
6. In principle, the elastic compressibility parameter C_p [equation (15)] can be determined from the volumetric stress–strain response immediately following a load reversal. However, due to intrinsic inaccuracies in these measurements, it is more reliable to measure the elastic shear wave velocity in either laboratory resonant column tests, or from field investigations using cross-hole or down-whole techniques (where knowledge of the current density and stress level is available). In this case C_b is estimated from G_{max}, μ'_0, and the initial void ratio and confining stress. For clean uniform sands, average values of $C_b = 800 \pm 100$, while for clays, C_b decreases as the plasticity index increases. Pestana[9] reports typical values, $C_b = 400$–500 for two low plasticity clays.
7. The parameter ω_s describes small strain (i.e. $\gamma \leqslant 0{\cdot}1$ per cent) non-linearity in shear and is evaluated through the analysis of shear modulus degradation with strain level. It is most reliably estimated from local strain measurements[61,62] in undrained triaxial tests on (lightly) overconsolidated test specimens.
8. Measurement of the critical state friction angle in triaxial compression shearing, ϕ'_{cs}, requires homegeneous distortion (i.e. no localization) of the test specimen at relatively large shear strains (in many cases, $\gamma > 10$–20 per cent). It is often difficult to measure this parameter for sands due to the development of shear bands (typically associated with strong dilation at low confining pressures). Reliable estimates of ϕ'_{cs} can be made from undrained shear tests performed on sand specimens that are consolidated in the (high pressure) LCC regime. For clean sands, Jamiolkowski *et al.*[63] report $\phi'_{cs} = 33{\cdot}5 \pm 2{\cdot}5^{\circ}$. The critical state friction angle for clays is usually well defined from undrained shear of K_0-normally consolidated specimens (at $\gamma \leqslant 15$ per cent).

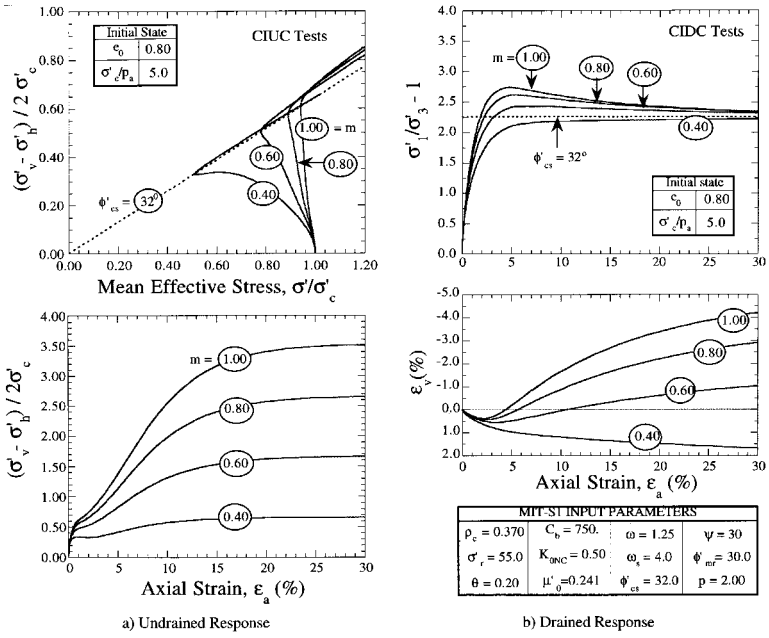

Figure 12. Effect of input parameter m behavior of a medium dense sand; (a) Undrained response; (b) Drained response

9. The parameters m, ϕ'_{mr} and p define the shape of the yield surface as a function of the maximum consolidation stresses and current void ratio:
   (a) For sands p and ϕ'_m can be found by a small parametric study to fit the predicted peak friction angles for two samples with different formation densities at a given confining stress. Limited experience show that values of p for clean uniform sands range between 2 and 3 with an average of $2{\cdot}5 \pm 0{\cdot}25$, while values of ϕ'_{mr} are highly dependent on ϕ'_{cs} and the practical limits of formation densities (i.e. e_{max}, e_{min}). The parameter m plays a dominant role in the shear behaviour of freshly deposited sands. For example, Figure 12 illustrates model predictions of undrained and drained triaxial compression rests (CIUC and CIDC) of a hypothetical medium-dense sand (formation void ratio, $e_0 = 0{\cdot}80$) at a given confining pressure stress ($p'/p_a = 5$). As the parameter m increases from 0·4 to 1·0, there is a large increase in the undrained shear strength, and a corresponding reduction in the shear-induced pore pressure ($\Delta u_s = -\Delta p'$) occurring at peak stress obliquity (Figure 12a, b). For drained shearing, increasing the value of m causes a transition from contractive behaviour to dilation associated with a peak shear strength. The parameter m can then be estimated by matching the computed and measured shear response in either undrained or drained shear tests. Limited experience suggests $m = 0{\cdot}55 \pm 0{\cdot}15$ for clean, relatively uniform sands.[9]
   (b) For clays with normalized shear strength properties, $p = 0$, while ϕ'_m and m can be selected by matching the model computations with measured effective stress paths for undrained shearing of K_0-normally consolidated specimens in triaxial compression and extension modes (i.e. CK_0UC; CK_0UE). Figure 13(a) shows the effects of selected pairs of

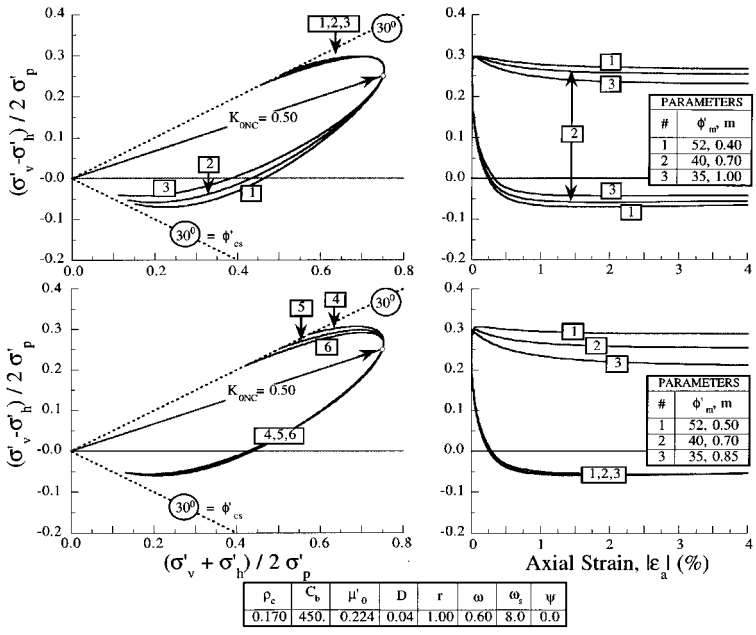

Figure 13. Effect of input parameters ϕ'_m and m in the undrained behaviour of K_0-consolidated clay specimens; (a) Matching undrained shear strength, (b) Matching initial behaviour in extension mode of shearing

parameters ϕ'_m and m to match undrained strength in triaxial compression. At nearly the same undrained strength, a higher value of m (and therefore a lower value of ϕ'_m) induces more softening in compression and an increase in pore pressure in extension. Figure 13(b) shows selected pairs of values for ϕ'_m and m giving nearly the same initial undrained response in extension. As the input parameter m increases the peak undrained strength in compression decreases and the simulations show an increased softening.

10. ψ is a dimensionless constant which controls the rate of change of anisotropy caused by the imposed strain (or stress) history. Figure 14 shows the effect of ψ in the predicted undrained and drained behaviour is triaxial compression tests for a medium dense sand. For undrained tests, increasing rotation rates show minimal effect on the predicted stress paths (limited to obliquities close to the transformation line- or characteristic state) and no effect on the ultimate strength or pore pressure, while the stress–strain curves are significantly affected by rotation rate (Figure 14a). For drained tests, as the rotation rate increases, the peak obliquity is reached at a smaller axial (shear) strain (e.g. at 5 per cent for ψ between 30 and 60 versus 12.5 per cent for $\psi = 5$) and the specimens exhibit slightly higher dilation rates with increasing values of ψ (Figure 14b). For drained and undrained shear tests, rotation rates in excess of 50–60 result only in marginal differences in the stress–strain curves, for the selected input parameters. Limited experience suggests values of ψ in the order of 50 (30–100). For clays, input parameter ψ is obtained from shear-induced pore pressures or stress–strain curves at relative large strains (ε_d = 5–10 per cent) in triaxial compression and/or extension tests. Figure 15 shows two key features of the model:

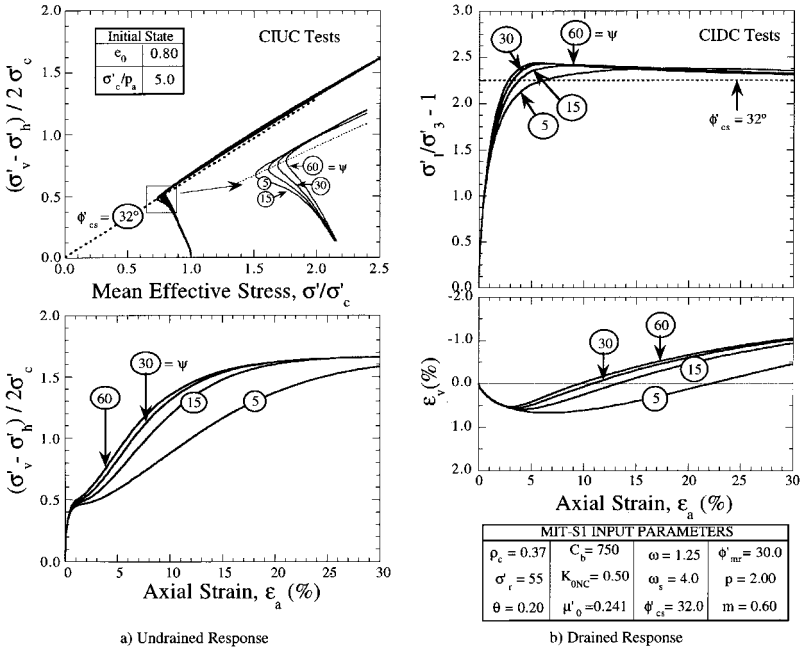

Figure 14. Effect of rate of evolving anisotropy, ψ, in the behaviour of isotropically consolidated sand specimens (a) Undrained response; (b) Drained response

(a) Changes in ψ do not affect significantly the effective stress paths in the compression mode while it is the primary factor controlling shear induced pore pressures (i.e. stressed paths) in extension; (b) Large strain conditions are independent of rotation rate (for $\psi \neq 0$), but these conditions are reached at lower shear strains as ψ increases.

Extensive parametric studies[9] have been carried out to identify practical methods for estimating ψ. In general, the parameter ψ has a significant impact on the predicted stress–strain response in undrained shear tests at moderate to large strain levels ($\gamma = 5$–20 per cent), and is most conveniently estimated from CIUC tests on medium–dense sands; or CK_0UE tests on K_0-normally consolidated clays.

In addition to the material constants, the model also requires initial values of all state variables to be defined, these comprise: (i) the effective stress tensor, σ', (ii) the void ratio, e, (iii) the size and orientation of the bounding surface, α' and $\mathbf{b}$, (iv) the effective stress state at the last stress reversal point (SRP), σ'_{rev}) the strains accumulated from the last SRP, ${}^{\Delta 1}\varepsilon$, and (vi) the size of the load surface at first yield, α_{0i} [equation (23c)]. All of the examples in this paper assume that the soil is freshly deposited at a specified void ratio, with the stress state located at the tip of the bounding surface (i.e. directions of the yield surface coincide with the applied stresses). All other state variables then assume default values ($\sigma'_{rev} = \sigma'$, ${}^{\Delta 1}\varepsilon = \mathbf{0}$, and $\alpha_{0i} = \alpha'$). Additional assumptions are required to estimate the initial state variables of in situ, overconsolidated soils and is outside the scope of this paper.

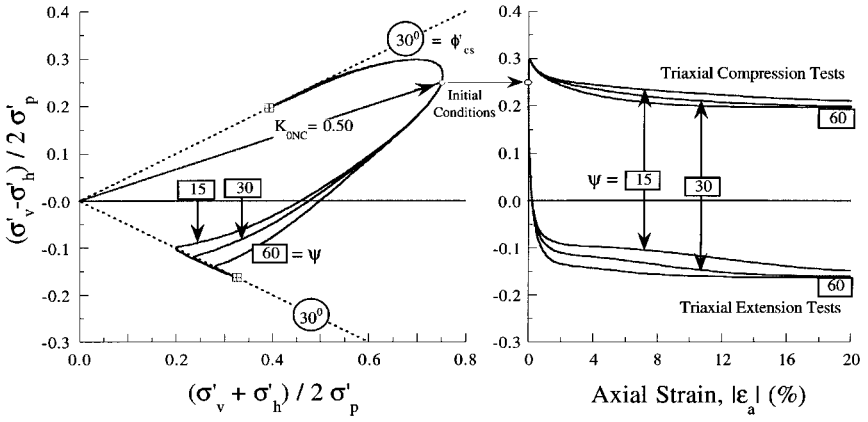

MIT-S1 INPUT PARAMETERS								
ρ_c	C_b	μ'_0	D	r	ω	ω_s	ϕ'_m	m
0.170	450.	0.224	0.04	1.00	0.60	8.0	40.0	0.70

Figure 15. Effect of rate of evolving anisotropy, ψ, in the undrained behaviour of K_0-consolidated clay specimens

4. CONCLUSIONS

This paper presents details of the formulation of a new effective stress soil for describing the rate independent behaviour of freshly deposited and overconsolidated soils. The new model uses the same basic structure as a previously reported protype, but introduces significant changes in the form of the bounding surface and hardening laws; while a new framework of compression behaviour unifies the modelling of clays and sands. The proposed model introduces new expressions for describing small strain non-linearity, thus enhancing predictions of shear modulus degradation for both clays and sands, and uses a variable Poisson's ratio to describe more realistically the variation of K_0 measured during one-dimensional swelling and subsequent reloading.

The model explicitly incorporates the current void ratio as a state variable, in addition to the stress state, to describe peak friction angles and dilation rates as a function of initial formation density in the transitional regime for sands. The proposed model uses a limited number of input parameters, that can all be derived from standard types of laboratory test. Companion papers present a complete model evaluation for sands and clays.[54,55].

ACKNOWLEDGEMENTS

The authors would like to acknowledge INTEVEP, S.A and the Gilbert W. Winslow Career Development Chair at MIT for supporting this research. The authors gratefully acknowledge the meticulous review by Ms Mao and Dr. Randolph from the University of Western Australia and Professor C.C. Ladd from MIT for many insightful comments during the elaboration of the initial manuscript.

APPENDIX I

List of symbols

The following symbols are used in this paper:

$a(\phi'_{cs})$	parameter defining LCC spacing at different stress ratios (i.e. σ'_h/σ'_v = constant)
$\mathbf{b}$	orientation tensor for bounding surface
c^2, c_a^2	scalar parameters defining the shape of the bounding surfaces
C_b	material constant describing small strain 'elastic' bulk modulus
D	material constant controlling 1-D swelling for clays
e, e_i, e_0	current, initial and formation void ratio, respectively
ε_s	tensor of deviatoric strains
$f(\sigma', e, \alpha', \mathbf{b})$	bounding surface for normally consolidated soils
g_1	mapping function for bounding surface plasticity
G, G_{max}, G_{sec}	current, maximum (i.e. at reversal) and secant shear modulus, respectively
$h_f(\eta)$	large strain (critical state) failure criterion
h	material constant controlling irrecoverable plastic strains in unload–reload cycles
H, H^I, H^0	current and elasto-plastic modulus at the image point for overconsolidated (OC) soil and at first yield, respectively
$\mathbf{I}$	identity tensor
$J_{3\eta}$	third invariant of the stress ratio tensor
k^2, k_a^2	scalar parameters defining critical state (large strain) conditions
K, K_{max}	tangent and maximum bulk modulus (i.e. at stress reversal), respectively
K_0	lateral earth pressure coefficient for zero lateral strain
K_{0NC}	K_0 value for normally consolidated clays and sands in the LCC regime
LCC	Limiting Compression Curve
m	material parameter describing slenderness of the bounding surface
OCR, OCR_1	overconsolidation ratio and OCR at $K_0 = 1$ during 1-D swelling, respectively
p	material constant describing change of bounding surface shape as a function of current void ratio
p'	mean effective stress
$\mathbf{P}$	directions of plastic strain increments (flow direction tensor)
P^0, P^I	direction of plastic flow at first yield for OC soils and at the image point, respectively
p_a	atmospheric pressure
$\mathbf{Q}$	gradient of bounding surface
r	material constant controlling non-linearity in 1-D swelling
r_x, r_y	scalar parameters describing rotational hardening of bounding surface
R, R_m	current and maximum mean effective stress ratio
$\mathbf{s}$	tensor of deviatoric stress
x	parameter describing K_0 conditions for 1-D consolidation of soils
α'	size of bounding surface
α'_0, α'_{0i}	size of load surface and load surface at first yield, respectively
δ_b	dimensionless distance of the current load surface to the corresponding LCC
$\Delta\varepsilon^p$, Δ^p	residual plastic strain and normalized residual plastic strain at the end of hydrostatic unload–reload cycle, respectively

$\varepsilon = \varepsilon_p \mathbf{I} + \varepsilon$	infinitesimal strain tensor
${}^{\Delta 1}\varepsilon$	accumulated strain since last stress reversal point
ε_a, γ	axial and shear strain, respectively
ϕ'_{cs}	critical state friction angle at large strains in triaxial compression tests
$\phi'_m(e)$	maximum friction angle describing bounding surface shape
ϕ'_{mr}	material constant defining maximum friction angle, ϕ'_m, at $e = 1$
η, η_{rev}	current and stress ratio tensor at stress reversal point, respectively
$\delta\lambda$	scalar controlling magnitude of plastic strain increments
μ'_0	Poisson's ratio at stress reversal controlling $2G_{max}/K_{max}$
θ	material constant describing transitional regime for freshly deposited sands
ρ_c	soil compressibility in the LCC regime
ρ_r	parameter defining the current elastic volumetric stiffness
σ'_v, σ'_c	vertical and confining effective stress, respectively
p'_{ref}, σ'_{vref}	reference mean and vertical effective stress at unity void ratio defining location of H-LCC and K_0-LCC, respectively
p'_{rev}	mean effective stress at stress reversal point
σ'	effective stress tensor
ξ, ξ_s	scalar distance parameters used in perfectly hysteretic model
ω, ω_s	material constants describing variable Poisson's ratio and small strain non-linearity in shear, respectively
χ	strain amplitude parameter
ψ	material constant controlling rate of rotation of bounding surface
ζ	scalar parameter describing current aperture of the bounding surface

APPENDIX II

Uniqueness of LCC's

Elastoplastic models which use an isotropic yield function and assume density hardening of the yield surface predict the location of the normally consolidated states for any stress ratio, η, from the geometry of the yield surface and the ratio of elastic to plastic compressibilities (e.g. Cam Clay family of models). For models with anisotropic yield surfaces and hardening rules to describe evolving anisotropy, the location of the LCC is no longer a function of the stress ratio but depends on the rate at which the anisotropy evolves. The proposed model introduces an isotropic spacing function, F, defined in terms of the internal variables, α', $\mathbf{b}$ which describe the size and orientation of the bounding surface, α'_e corresponding to the value of the mean effective stress at the hydrostatic LCC for the current void ratio (i.e. Figure 1); and parameter 'a' describing the shape of the spacing function:

$$F\left(\frac{\alpha'}{\alpha'_e}, \mathbf{b}, a\right) = 0 \tag{26}$$

From the consistency condition, the internal state $(\alpha', \mathbf{b})$ must remain in contact with the spacing function, F:

$$\mathrm{d}F = 0 = \frac{\partial F}{\partial(\alpha'/\alpha'_e)}\,\delta\left(\frac{\alpha'}{\alpha'_e}\right) + \frac{\partial F}{\partial \mathbf{b}} : \delta\mathbf{b} + \frac{\partial F}{\partial a}\,\delta a = 0 \tag{27}$$

Assuming that the shape of the spacing function remains constant ($\delta a = 0$) and rearranging terms, it is possible to obtain

$$\frac{\delta\alpha'}{\alpha'} = \frac{\delta\alpha'_e}{\alpha'_e} - \left(\frac{\alpha'_e}{\alpha'}\right)\frac{\partial F/\partial \mathbf{b} : \delta\mathbf{b}}{\partial F/\partial \alpha'} = 0 \tag{28}$$

Equation (28) represents the general expression providing coupling between density and kinematic hardening and guarantees uniqueness of the LCC for models using anisotropic yield surfaces with kinematic hardening rules. For no further rotation, $\delta b = 0$ (e.g. full re-orientation of the yield surface) we obtain

$$\delta\alpha'/\alpha' = \delta\alpha'_e/\alpha'_e \tag{29}$$

Solution to this equation (i.e. $\mathrm{d}[\ln(\alpha')] = \mathrm{d}[\ln(\alpha'_e)]$) results in parallel lines in any logarithmic space for α' and α'_e (i.e. e-$\ln\sigma'$; $\log(1+e)$-$\log p'$; $\log e$–$\log p'$) The proposed model assumes that the function F is an isotropic ellipse (i.e. similar to MCC) defined by the critical state friction angle in compression, ϕ'_{cs}:

$$F = \mathbf{b} : \mathbf{b} - a^2\left(\frac{\alpha'_e}{\alpha'} - 1\right) = 0, \quad \text{where } a^2 = 24\left(\frac{\sin\phi'_{cs}}{3 - \sin\phi'_{cs}}\right)^2 \leqslant 1 \tag{30}$$

Equation (30) controls the spacing of LCC for different stress ratios and it describes the separation of the LCC for hydrostatic and K_0 compression (c.f. Figure 5). Substituting equation (30) into equation (28), we obtain:

$$\frac{\delta\alpha'}{\alpha'} = \frac{\delta\alpha'_e}{\alpha'_e} - \frac{2\mathbf{b} : \delta\mathbf{b}}{a^2 + b : \mathbf{b}} = 0 \tag{31}$$

Expression (31) generalizes the expression of density hardening developed from hydrostatic compression tests to non-hydrostatic stress conditions and provides coupling between size hardening and kinematic hardening for the MIT-S1 model.

REFERENCES

1. A. J. Whittle and M. J. Kavvadas, 'Formulation of MIT-E3 constitutive model for overconsolidated clays', *J. Geotech Engng., ASCE*, **120**(10), 173–198 (1994).
2. A. J. Whittle, D. J. DeGroot, C. C. Ladd and T.-H. Seah, 'Model prediction of anisotropic behaviour of Boston Blue Clay', *J. Geotech. Engng., ASCE*, **120**(1), 199–224 (1994).
3. A. J. Whittle, Y. M. A. Hashash and R. V. Whitman, 'Analysis of a deep excavation in Boston', *J. Geotech. Engng., ASCE*, **119**(1), 69–91 (1993).
4. C. C. Ladd, A. J. Whittle and D. E. Legaspi, 'Stress-deformation behavior of an embankment on Boston Blue Clay', *Vertical and Horizontal Deformations of Foundations and Embankments*, ASCE Geotechnical Special Publication No. **40**(2), 1730–1759 (1994).
5. D. C. Drucker, R. E. Gibson and D. J. Henkel, 'Soil mechanics and work hardening theories of plasticity', *Trans. Am. Soc. Civ. Engrs.* **122,** 338–346 (1957).
6. A. Casagrande, 'Characteristics of cohesionless soils affecting the stability of slopes and earth fills', *J. Boston Soc. Civ. Engrs.* **23**(1), 13–32 (1936).
7. L. Rendulic, 'Relation between void ratio and principal effective stresses for a remoulded silty clay', *Proc. 1st Int. Conf. Soil Mechs. & Found. Engng.*, Harvard, 3, D-27, 1936.
8. C. C. Ladd and R. Foott, 'New design procedure for stability of soft clays', *J. Geotech Engng. Div., ASCE*, **100** (GT7), 763–786 (1974).
9. J. M. Pestana, 'A unified constitutive model for clays and sands', *Sc.D. Thesis*, Department of Civil & Environmental Engineering, Massachusetts Institute of Technology, Cambridge, MA, 1994.

10. N. Yasufuku, H. Murata, M. Hyodo and A. F. L. Hyde, 'A stress–strain relationship for anisotropically consolidated sand over a wide stress region', *Soils Found*., **31**(4), 75–92 (1991).
11. S. Somasundaram and C. S. Desai, 'Modelling and testing for anisotropic behavior of soils,' *J. Geotech. Engng*. **119**(4), 714–748 (1993).
12. D. Kolymbas, I. Herle and P. A. Von Wolffersdorff, 'Hypoplastic constitutive equation with internal variables', *Int. J. Numer. Anal. Meth. Geomech*., **19**(6), 415–436 (1995).
13. K. Been and M. G. Jefferies, 'A state parameter for sands', *Géotechnique*, **35**(2), 99–112 (1985).
14. M. G. Jefferies, 'Nor-Sand: a simple critical state model for sand', *Géotechnique*, **43**(1), 91–103 (1993).
15. K. Been, M. G. Jefferies and J. Hachey, 'The critical state of sands', *Géotechnique* **41**(3), 365–381 (1991).
16. R. S. Crouch, J. P. Wolf and Y. F. Dafalias, 'Unified critical state bounding surface plasticity model for soil', *J. Engng. Mech., ASCE* **120**(11), 2251–2270 (1994).
17. P. V. Lade, 'Elasto-plastic stress–strain theory for cohesionless soil with curved yield surfaces', *Int. J. Solids Struct*. **13,** 1019–1035 (1977).
18. K. Nishi and Y. Esashi, 'Elasto-plastic model of fully saturated sand under undrained static and cyclic loading', *Proc. 4th Int. Conf. on Numer. Methods in Geomech*., Edmonton, Vol. I, 1982, pp. 235–244.
19. J. R. F. Arthur and B. K. Menzies, 'Inherent anisotropy in a sand', *Géotechnique*, **22**(1), 115–128.
20. M. J. P. R. Symes, 'Rotation of principal stresses in sand', *Ph.D. Thesis*, Dept. of Civil Engng., Imperial College, University of London, (1983).
21. V. N. Georgiannou, D. W. Hight and J. B. Burland, 'Undrained behaviour of natural and model clay sands', *Soils Found*., **31**(3), 17–29 (1991).
22. N. Yasufuku, H. Murata and M. Hyodo 'Yield characteristics of anisotropically consolidated sand under low and high stresses', *Soils Found*., **31**(1), 95–109 (1991).
23. J. M. Pestana and A. J. Whittle, 'Compression model for cohessionless soils', *Géotechnique*, **45**(4), 611–631 (1995).
24. N. Miura, H. Murata and N. Yasufuku, 'Stress–strain characteristics in a particle-crushing region', *Soils Found*. **24**(1), 77–89 (1984).
25. P. V. Lade and J. A. Yamamuro, 'Undrained sand behavior in axisymmetric tests at high pressures', *J. Geotech. Engng., ASCE*, **122**(2), 120–129 (1996).
26. C. S. Desai, S. Somasundaram and G. Frantziskonic, 'A Hierarchical approach for constitutive modeling of geologic materials', *Int. J. Numer. Anal. Meth. Geomech*., **10**(3), 225–257 (1986).
27. C. S. Desai, 'Unified approach for constitutive modelling for geologic materials and discontinuities', *Proc. 6th Int. Conf. on Numerical Methods in Geomechanics, Swoboda, Ec., Innsbruck*, 1988, pp. 45–54.
28. D. R. Katti and C. S. Desai 'Modelling and testing of cohesive soils using the Disturbed State Concept', *J. Geotech. Engng., ASCE*, **21**(5), 648–658 (1995).
29. S. Armaleh and C. S. Desai 'Modelling and testing of a cohesionless soil using the Disturbed State Concept', *Int. J. Meth. Behavior of Mater*., **5**(3), 279–295 (1994).
30. J. H. Prévost, 'Plasticity theory for soil stress–strain behaviour', *J. Engng. Mech., ASCE*, **104**(EM5), 1177–1194 (1978).
31. H. Matsuoka and T. Nakai, 'Stress-deformational and strength characteristics under three different principal stresses', *Proc. Japanese Soc. Civ. Engrs*., **232,** 59–70 (1974).
32. J. M. Pestana and A. J. Whittle, 'Model prediction of anisotropic clay behaviour due to consolidation stress history', *Proc. 8th Int. Conf. on Computer Methods and Advances in Geomechanics* (IACMAG '94), Morgantown, WVa., Vol. 2, 1994, pp. 1527–1532.
33. K. H. Roscoe and J. B. Burland, 'On the generalized stress–strain behaviour of 'wet' clay', in J. Heyman and F. A. Leckie (eds), *Engineering Plasticity*, Cambridge University Press, Cambridge, 1968, pp. 535–609.
34. A. Gens, 'Stress–strain and strength of a low plasticity clay', *Ph.D. Thesis*, Dept. of Civil Engineering, Imperial College, University of London, 1982.
35. A. J. Hendron Jr., 'The behavior of sand in one-dimensional compression', *Ph.D. Thesis*, University of Illinois at Urbana 1963.
36. A. S. Vesic, 'Creating by explosives as an earth pressure problem', *Proc. 6th Conf. on Soil Mechs. & Found. Engng*., Montreal, 1965, Vol. II, pp. 427–431.
37. M. D. Bolton, 'The strength and dilatancy of sand', *Géotechnique*, **36**(1), 65–78 (1986).
38. P. A. Vermeer, 'A double hardening model for sand', *Géotechnique*, **28**(4), 413–433 (1978).
39. K. Hashiguchi, 'An expression of anisotropy in a plastic constitutive equation of soils', *Proc. 9th Int. Conf. on Soil Mechs. & Found. Engng*., Tokyo, 1977, pp. 302–305.
40. C. C. Ladd and L. Edgers, 'Consolidated-undrained direct simple shear tests on Boston blue clay', *Research Report R72-82*, Department of Civil Engineering, MIT, Cambridge, MA, 1972.
41. A. Gens, 'Discussion, *Proc. 7th European Conf. on Soil Mechs. & Found. Engng., Brighton*, Vol. **4,** 25–26.
42. M. Oda, 'The mechanism of fabric changes during compressional deformation of sand', *Soils Found*. **12**(2), 1–18 (1972).
43. R. Nova and D. M. Wood, 'A constitutive model for sand in triaxial compression', *Int. J. Numer. Anal. Meth. Geomech*., **3**(3), 255–278 (1979).
44. K. L. Lee and I. Farhoomand, 'Compressibility and crushing of granular soil in anisotropic triaxial compression', *Can. Geotech. J*., **4**(1), 68–86 (1969).

45. M. R. Coop, 'The behavior of granular soils at elevated stresses', in G. T. Houlsby and A. N. Schofield (eds), *Predictive Soil Mechanics*, *Proc. Worth Memorial Symposium*, Oxford, 1992, pp. 186–199.
46. S. Banerjee, R. Davis and K. Sribalaskandarajah, 'Simple double hardening model for geomaterials', *J. Geotech. Engng., ASCE*, **118**(6)**,** 889–901 (1992).
47. T. Hueckel and R. Nova, 'Some hysteresis effects of the behaviour of geological media', *Int. J. Solids Struct.* **15,** 625–642 (1979).
48. Y. F. Dafalias and L. R. Herrmann, 'Bounding surface formulation of soil plasticity', in G. N. Pande and O. C. Zienkiewicz (eds), *Soil Mechanics*: *Transient and Cyclic Loads*, chapter 10, Wiley, New York, 1982, pp. 253–282.
49. G. T. Houlsby, 'The use of a variable shear modulus in elastic–plastic models for clays, *Comput. Geotech.*, **1**(1)**,** 3–13 (1985).
50. B. Loret and M. P. Loung, 'A double deformation mechanism for sand', *Proc. 4th Int. Conf. on Numer. Methods in Geomech.*, Vol. **1,** 197–206.
51. P. V. Lade and R. B. Nelson, 'Modelling the elastic behaviour of granular materials', *Int. J. Numer. Anal. Meth. Geomech.* **11,** 521–542 (1987).
52. H. B. Seed, R. T. Wong, I. M. Idriss and K. Tokimatsu, 'Moduli and damping factors for dynamic analyses of cohesionless soils', *Report UCB/EERC-84/14*, University of California, Berkeley, 1984.
53. J. I. Sun, R. Golesorkhi and H. B. Seed 'Dynamic moduli and damping ratios for cohesive soils', *Report UCB/EERC-88/15*, University of California, Berkeley, 1988.
54. J. M. Pestana, A. J. Whittle, 'Evaluation of a unified constitutive model for clays and sands: I—sand Behavior', *Int. J. Numer. Anal. Meth. Geomech.*, submitted (1999).
55. J. M. Pestana and A. J. Whittle, 'Evaluation of a unified constitutive model for clays and sands: II—clay Behavior', *Int. J. Numer. Anal. Meth. Geomech.*, submitted (1999).
56. G. R. Andersen, 'Physical mechanisms controlling the strength and deformation behavior of frozen sand', *Ph.D. Thesis*, Department of Civil & Environmental Engineering, Massachusetts Institute of Technology,Cambridge, MA, 1991.
57. R. S. Ladd, 'Use of electrical pressure transducers to measure soil pressure', *SM Thesis*, Department of Civil Engineering, Massachusetts Institute of Technology, Cambridge, MA, 1966.
58. P. W. Mayne and F. H. Kulhawy, 'K_0-OCR relationships in soils', *J. Geotec. Engng*, *ASCE*, **108**(6)**,** 851–82.
59. G. Mesri and T. M. Hayat, 'The coefficient of earth pressure at rest', *Can. Geotech. J.*, **30**(3)**,** 647–666 (1993).
60. M. Jamiolkowski, R. Lancellotta, D. C. F. Lo Presti and O. Pallara, 'Stiffness of Toyoura sand at small and intermediate strain', *Proc. 13th Int. Conf. on Soil Mechs. & Found. Engng.*, New Delhi, India, 1994, pp. 169–172.
61. R. J. Jardine, M. J. P. R. Symes and J. B. Burland, 'The measurement of soil stiffness in the trial apparatus', *Géotechnique*, **34**(3)**,** 323–340 (1984).
62. F. Tatsuoka, T. Sato, C.-S. Park, Y.-S. Kim, J. N. Mukabi and Y. Kohata, 'Measurements of elastic properties of geomaterials in laboratory compression tests', *ASTM Geotech. Testing J.*, **17,** 80–94 (1994).
63. M. Jamiolkowski, V. N. Ghionna, R. Lancellota and E. Pasqualini, 'New correlations of penetration tests for design practice', *Proc. 1st Int. Symposium on Penetration Testing*, Orlando, Vol. I, 1988, pp. 263–296.
64. K. Ishihara, 'Liquefaction and flow failure during earthquakes', *Géotechnique*, **43**(3)**,** 351–415 (1993).

